Modal Acoustic Velocimetry in libration-driven flows - Part 2 : Inversion

Henri-Claude Nataf[1*] and Sylvie Su[2]

[1*]Univ. Grenoble Alpes, CNRS, IRD, Univ. Gustave Eiffel, ISTerre, 38000, Grenoble, France.
[2] Normandie Univ, UNIROUEN, INSA Rouen, CNRS, CORIA, 76000, Rouen, France.

*Corresponding author(s). E-mail(s): Henri-Claude.Nataf@univ-grenoble-alpes.fr;
Contributing authors: sylvie.su@univ-rouen.fr;

Abstract

Modal Acoustic Velocimetry consists in mapping fluid flow in a container from the modifications of its acoustic resonances it induces. In a companion article (Nataf et al. 2025), we presented measurements of 53 acoustic mode frequency 'splittings' produced by a libration-induced flow. The present article aims at recovering models of this flow through the inversion of the splitting data. We apply the SOLA inversion method, often used in helioseismology. Our data constrain the azimuthally-averaged fluid rotation rate. Both 1D- and 2D-inversions are performed. We know that the linear flow model of Greenspan (1968) gives a good account of the observed splittings. The inversions recover the main characteristics of this time-dependent flow. The 2D-inversion confirms the invariance of the flow along the rotation axis. Resolution kernels show that flow can be mapped on patches that spread over $\sim$ **5%** of a meridian quarter-plane.

Keywords: Modal Acoustic Velocimetry, libration, spheroid, acoustics, SOLA

1 Introduction

In a companion article entitled 'Modal Acoustic Velocimetry in libration-driven flows - Part 1 : Acquisition strategies' (Nataf et al. 2025), noted 'Paper 1' in the following, we presented different strategies to acquire the frequency splitting of acoustic doublets in a gas-filled rotating spheroid subject to longitudinal libration, expressed as:

$$f_{shell}(t) = f_o + \Delta f \sin(2\pi f_{lib} t). \tag{1}$$

Such splittings were measured for 53 ${}_nS_l^{\pm m}$ acoustic 'doublets' at several different phases of the periodic libration flow. The present article aims at recovering flow properties from these measurements.

1.1 Modal Acoustic Velocimetry for libration flows

How to obtain flow maps from the acoustic doublets' frequency splittings measured by Modal Acoustic Velocimetry (MAV)? Let us first recall that such a splitting can be produced both by the Coriolis acceleration (Ledoux 1951) and by fluid flow within the container (Aerts et al. 2010). Only the axisymmetric azimuthal component of flow velocity can be retrieved. Our goal is thus to obtain 2D meridional maps of axisymmetric fluid azimuthal velocity (or fluid rotation rate f_{fluid}).

Greenspan's linear theory of longitudinal libration in rapidly rotating spheroids indicates that this velocity component largely dominates the flow, except in a very thin Ekman layer beneath the container wall, where fluid experiences large meridional velocities (Greenspan 1968). In the experiments we performed, the thickness of the Ekman layer is less than 0.5mm, to be compared with the 0.20m equatorial radius of the spheroid. The theory also reveals that the flow organizes itself in concentric cylinders aligned with the rotation axis. Fluid azimuthal velocity thus only depends upon cylindrical radius s. Therefore a 1D inversion should also provide a good fit to the measured frequency splittings.

We have shown in Paper 1 that convolving Greenspan's flow with acoustic splitting kernels provides predicted frequency splittings that closely match the measured ones, apart for a small systematic time delay. This offers a good opportunity for assessing how well Modal Acoustic Velocimetry resolves and constrains fluid flow in actual experiments. Note that there is a linear relationship between mode frequency splitting and fluid rotation rate.

1.2 Flow velocity kernels

Once a collection of mode splittings is available, the next step is to invert these splittings to retrieve the flow velocity field. Let us first recall the relationship between the measured splittings and the fluid rotation rate. Given the properties of rapidly spinning fluids, we consider two coordinate systems: a classical (r, θ) system, with θ the colatitude and r the radius, and an (s, z) system with s the cylindrical radius, and z the coordinate along the spin axis. All lengths are normalized by the inner radius of the shell $r_o = \sqrt[3]{r_{eq}^2 r_{pol}} = 0.1966$ m.

1.2.1 2D kernels

Following Triana et al. (2014), we express the difference ${}_n\delta f_l^m$ between the frequencies of singlets ${}_nS_l^{-m}$ and ${}_nS_l^m$ as a function of the rotation rate $f_{fluid}(r, \theta)$ of the axisymmetric flow by:

$$ {}_n\delta f_l^m = 2m \int_0^1 \int_0^\pi {}_nK_l^m(r,\theta) f_{fluid}(r,\theta)\, r dr d\theta, \tag{2} $$

where sensitivity kernel ${}_nK_l^m(r,\theta)$ is given by:

$$ {}_nK_l^m(r,\theta) = \frac{r\sin\theta}{{}_nI_l}\left\{\xi_r^2 p^2 + \xi_h^2\left[q^2 + \frac{m^2}{\sin^2\theta}p^2 - 2\frac{pq}{\tan\theta}\right] - 2\xi_h\xi_r p^2\right\}, \tag{3} $$

with:

$$ p = P_l^m(\cos\theta), \quad q = \frac{dP_l^m(\cos\theta)}{d\theta}, \quad \xi_r = \frac{d\left[{}_nR_l(r)\right]}{dr} \text{ and } \xi_h = \frac{{}_nR_l(r)}{r}, \tag{4} $$

and ${}_nI_l$ a normalization integral:

$$ {}_nI_l = \int_0^1 \left[|\xi_r(r)|^2 + l(l+1)|\xi_h(r)|^2\right] r^2\, dr. \tag{5} $$

$P_l^m(\cos\theta)$ is the associated Legendre polynomial, and the radial eigenfunction ${}_nR_l(r)$ equals the spherical Bessel function of the first kind j_l evaluated at ${}_nk_l\, r$:

$$ {}_nR_l(r) = j_l({}_nk_l\, r), \tag{6} $$

with ${}_nk_l$ such that $\xi_r(1) = 0$ (no radial wave displacement at the solid shell boundary).

Note that all kernels are positive and symmetrical with respect to the equator of the reference frame. Although we compute mode frequencies to the second order in ellipticity, we stick to kernels of the sphere in our inversions. A method for computing pressure fields at higher-order in ellipticity in presented in Albo et al. (2010).

The 2D sensitivity kernels ${}_nK_l^m(r,\theta)$ of the collection of 53 modes discussed in this article are displayed in Appendix A.

1.2.2 1D kernels

Since Greenspan's flow is z-invariant, we integrate (r,θ) mode splitting kernels over z to get ${}_n\mathbb{K}_l^m(s)$ sensitivity kernels, in order to recover $f_{fluid}(s)$. We first express the 2D (r,θ) kernels in the (s,z) reference frame:

$$ {}_n\mathcal{K}_l^m(s,z) = {}_nK_l^m(r = \sqrt{s^2+z^2}, \theta = \arctan(s/z)). \tag{7} $$

We then integrate over z to obtain the 1D ${}_n\mathbb{K}_l^m(s)$ sensitivity kernels:

$$ {}_n\mathbb{K}_l^m(s) = \int_{-h(s)}^{h(s)} {}_n\mathcal{K}_l^m(s,z)\, dz \text{ with } h(s) = \sqrt{1-s^2}, \tag{8} $$

which provides the frequency splitting ${}_n\delta f_l^m$ of acoustic doublet ${}_nS_l^{\pm m}$ through:

$$ {}_n\delta f_l^m = 2m \int_0^1 {}_n\mathbb{K}_l^m(s) f_{fluid}(s)\, ds. \tag{9} $$

Figure 1 displays the 1D sensitivity kernels ${}_n\mathbb{K}_l^m(s)$ as a function of dimensionless cylindrical radius s for the collection of modes analyzed in this article. Note that kernels are not sharply localized and that sensitivity to fluid flow is obtained for $0.2 \lesssim s/r_o \lesssim 0.9$, all kernels dropping to 0 at $s/r_o = 0$ and $s/r_o = 1$.

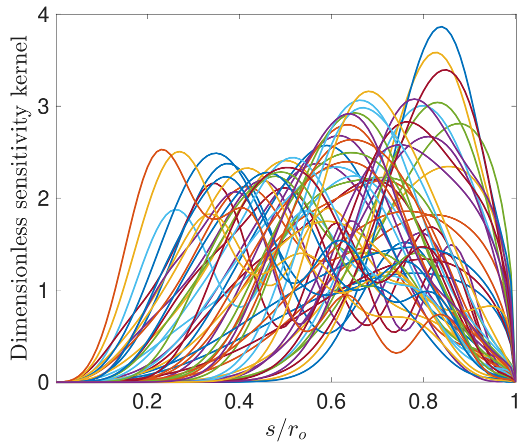

Fig. 1 Plot of 1D sensitivity kernels ${}_n\mathbb{K}_l^m(s)$ as a function of dimensionless cylindrical radius s for the collection of 53 acoustic doublets ${}_nS_l^{\pm m}$ analyzed in this article.

1.3 Tuning for libration flows

Here, we aim at recovering the libration-induced flow rotation rate in the frame of the spinning shell. This is why we corrected measured frequency splittings from the Coriolis splitting computed for the instantaneous spin rate of the shell. We can then use the kernels presented in the previous section to obtain f_{fluid} in the shell reference frame.

1.4 Inversion methods

Many inversion methods can be used for solving our linear problem. We will not review the vast literature on this topic, but only recall a few methods used in previous MAV studies. Two different methods were used in the seminal paper of Triana et al. (2014): a Tikhonov regularization and a semi-spectral Bayesian inversion. The former minimizes the second spatial derivatives of the flow velocity, while the latter relies on spherical harmonics to deal with the latitudinal flow variation, while a Bayesian approach is taken for its radial variation. A critical assessment of both methods is given by Mautino (2016) who reviews several alternatives. He also stresses that, considering the limited number of modes used in these early studies, the choice of the model smoothness parameters plays a major role, a concern shared by Su (2020) who used the semi-spectral Bayesian algorithm.

1.4.1 SOLA inversion

In order to better assess the intrinsic resolving power of a given data set of acoustic splittings, it seems appropriate to turn to 'Optimally Localized Averages' (OLA) inversion methods, pioneered by Backus and Gilbert (1967). These methods have recently gained a renewed interest in seismology (Zaroli 2019), and are widely used in helioseismology since the seminal papers of Pijpers and Thompson (1992, 1994). The idea of this class of methods is to extract from the data the best unbiased value of model parameters at a given location, or more precisely within a given volume around the target location. Two variants stand out: 'Multiplicative Optimally Localized Averages' (MOLA) and 'Subtractive Optimally Localized Averages' (SOLA).

The results of this article are obtained using the SOLA inversion method, closely following the detailed prescriptions of Zaroli (2019). Appendix B provides a summary of SOLA's procedure and notations. In our 2D SOLA inversions, we target disks of a given radius in the meridional plane, while our targets are s-segments in our 1D inversions.

The main drawback of OLA inversion methods is that they only target a few selected spots of model space. Hence, they do not provide a complete continuous 'best' model. This prevents computing the resulting best fitting data, to be compared with the original data with their error bars. In the simple examples we show, we circumvent this limitation by targeting enough spots in model space. A smooth continuous model is then built by interpolation/extrapolation, from which synthetic data of the inverted model can be computed.

Although OLA methods are often presented as 'parameter-free', they involve a 'trade-off' parameter η, which governs the ratio between resolution misfit and model variance (see equation B1). The choice of η can be made to obtain a normalized misfit close to 1. Since we observe that Greenspan's flow provides a very good fit to our splitting data, we can double check that the chosen 'trade-off' parameter provides flows that respect the smoothness of Greenspan's flow, given the collection of mode splittings we retrieve, and the precision of the measurements.

We present the ingredients and the results of a 1D SOLA inversion in Section 2, and of a 2D SOLA inversion in Section 3, both for a selected libration run with $f_o = 15$ Hz, $f_{lib} = 0.05$ Hz and $\Delta f = 1.5$ Hz (see Paper 1 for explanations). Limitations and perspectives are given in Section 4, and we conclude with Section 5.

2 1D SOLA flow inversion

Since we do expect libration flow to be largely z-invariant, we start with 1D SOLA inversions. In Paper 1, we obtained the frequency splitting of a collection of 53 acoustic doublets for 10 different phases of the periodic libration flow. Due to our acquisition strategy, the sampled libration phases are different for different modes. For all modes, the variation of the frequency splitting with libration phase is well fit by a sine. We thus use this sine pattern to interpolate our measurements to a set of 10 fixed libration phases from 0° to 324° in 36° steps. We attribute to each interpolated splitting an error equal to the mean of the 10 (or less) estimated errors for the considered measurements for each mode. An inversion of the 53 acoustic splittings is performed for each of the 10 selected libration phases. Note that although 10 independent inversions are computed, the data they invert correspond to the phases of a single sinusoidal fit of each mode.

2.1 Fluid rotation rate profiles

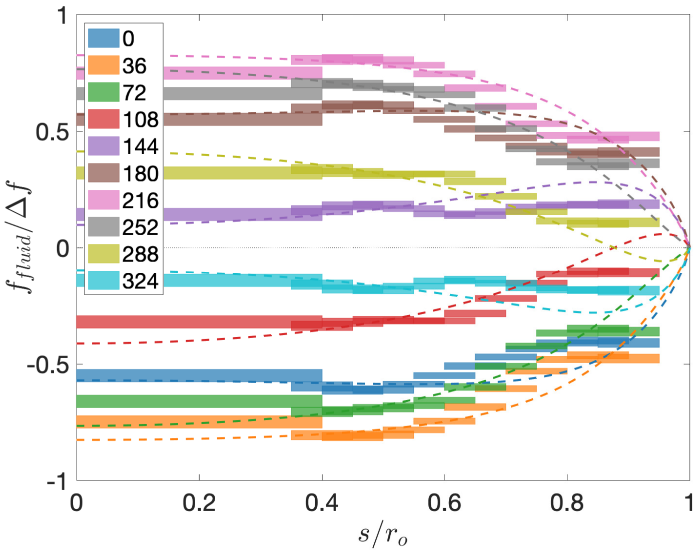

Fig. 2 1D SOLA inversion results for libration flow ($f_o = 15$ Hz, $f_{lib} = 0.05$ Hz and $\Delta f = 1.5$ Hz): normalized fluid rotation rate as a function of dimensionless cylindrical radius for 10 libration phases (legend in degrees). The width of the color boxes gives the targets' width, while their height is the inversion error. The color dashed lines are the predictions from Greenspan's flow at each libration phase delayed by 10°.

Figure 2 gathers the fluid rotation rate $f_{fluid}(s)$ s-profiles obtained from the inversions at 10 libration phases. The width of each box gives the target's width, while its height is the error estimate of the inverted model for this target. For comparison, we draw the profiles predicted by Greenspan's linear theory. In Paper 1, we pointed out that the measured splittings appear to be late by a few tenths of a second, probably because our acquisition strategy does not account for the time it takes for an acoustic mode to build up. Therefore, we add a phase-delay of 10° (corresponding to 0.56s) to the synthetics.

For this inversion, we chose $\eta = 40$. The amplitudes and trends of the theoretical profiles are well retrieved in our inversion. However, the gentle decrease of f_{fluid} with

s between $s = 0.7$ and $s = 1$ is not correctly retrieved. We will discuss the reasons for this disagreement in section 4, where we also explore the effect of different values of η.

2.2 Resolution kernels

An advantage of the SOLA inversion method is that it emphasizes the actual resolving power of the data, in a more objective way than other methods.

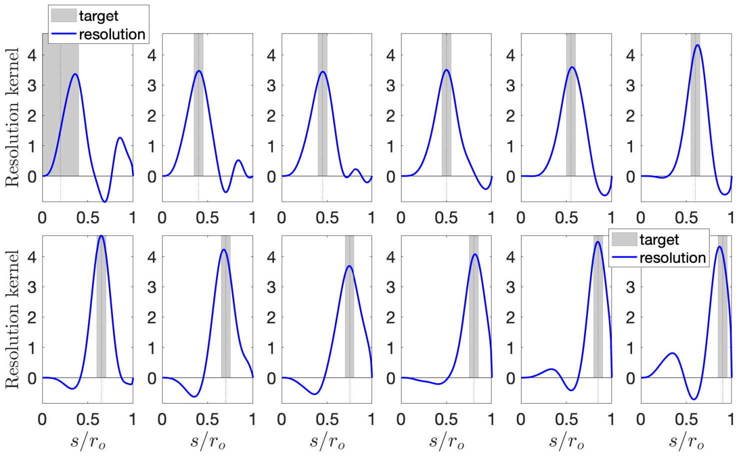

Fig. 3 Resolution kernels $A^{(k)}(s)$ for the 1D SOLA inversion of the splittings of 53 acoustic doublets. For each of the 12 targets, the resolution kernel is plotted as a function of dimensionless cylindrical radius, on top of a gray-shaded vertical band that gives the position and width of the target.

Figure 3 plots the resolution kernels $A^{(k)}(s)$ for the 12 s-segments we target. All resolution kernels appear well peaked around the target, except for the target near the center axis ($s/r_o = 0.4$). Low scores in these regions are expected, since all MAV flow kernels vanish on the axis (see Figure 1). Negative lobes present for most kernels indicate that the estimate of the flow rotation rate we retrieve is not perfectly 'unbiased'. We also note that the width of the resolution kernels at mid-height is at least twice as large as the targets' width.

2.3 Data fits

We now examine the fit to the data achieved by our inverted 1D models. Remember that the SOLA method only provides the best model estimate at targets. We need a complete s-profile to compute the predicted frequency splittings of the acoustic doublets we inverted. We use MATLAB®'s modified Akima (Akima 1970) interpolation method to construct a smooth $f_{fluid}(s)$ curve, imposing $f_{fluid} = 0$ at $s = 1$. We can thus compare the measured frequency splittings, with their error bars, to the splittings predicted by our best model. Figure 4 shows such a comparison for a libration phase of 180°. We see that our model can explain almost all measurements within their error

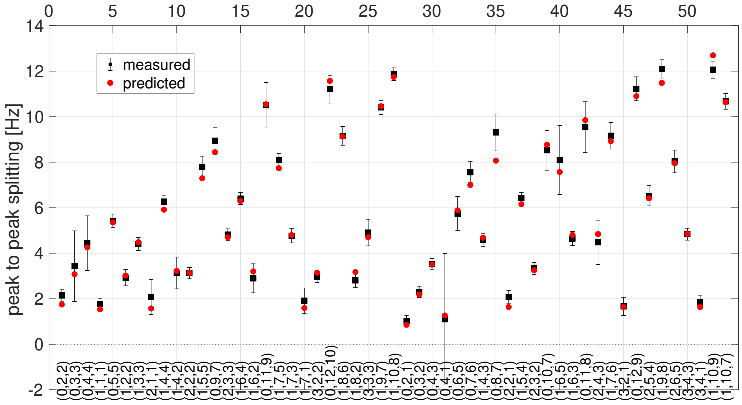

Fig. 4 Measured peak-to-peak frequency splitting [Hz] of our collection of 53 acoustic doublets for a libration phase of 180°, with their error bars (black symbols). The red symbols are the splittings predicted from a smoothed s-profile of f_{fluid} of our inverted model (grey-shaded targets in Figure 3). The (n, l, m) indices of the modes are indicated beneath the x-axis.

bars, with an average normalized misfit $misfit \simeq 0.73$, where $misfit$ is defined as:

$$misfit = \sqrt{\left\langle \left(\frac{\delta f_{pred} - \delta f_{meas}}{\sigma} \right)^2 \right\rangle}, \tag{10}$$

in which δf_{meas} is the measured splitting of a given doublet, σ is its error bar, and δf_{pred} is the splitting predicted by the inverted model for the same mode. The average is performed over the 53 doublets of our collection.

3 2D SOLA flow inversion

We now turn to a 2D inversion, with the goal of examining how well our mode collection constrains the z-invariance of fluid flow that characterizes Greenspan's asymptotic solution. We thus use the 2D kernels presented in section 1.2.1 to invert the same collection of 53 splittings and retrieve $f_{fluid}(r, \theta)$ at selected (r, θ) targets.

3.1 Fluid rotation rate maps

We chose 64 targets that cover most of an (r, θ) quarter-plane, as depicted in Figure 5. Remember that one can only retrieve flows that are symmetrical with respect to the equator. Targets are placed on an (s, z) grid, so that we can draw smoothed s-profiles of f_{fluid} at different z, as depicted in Figure 5c. The targets are disks, with radius equal to 0.025, except for the z-column at $s = 0.25$, where we chose a radius of 0.075, anticipating the poor spatial resolution we expect near the axis.

Figure 5 displays the results we obtain for a libration phase of 180°, with $\eta = 40$. Inverted $f_{fluid}/\Delta f$ at target locations are given in 5a, with an error shown in Figure

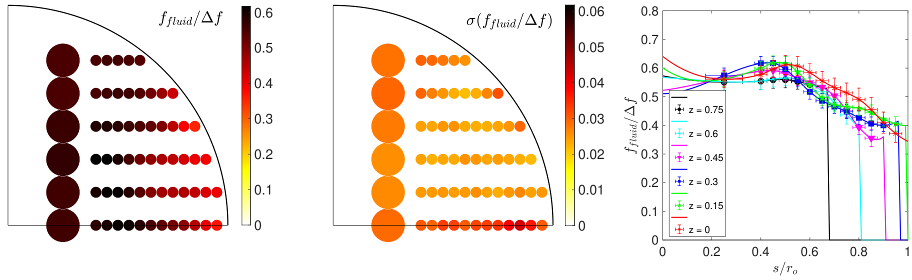

Fig. 5 2D SOLA inversion results for libration flow ($f_o = 15$ Hz, $f_{lib} = 0.05$ Hz and $\Delta f = 1.5$ Hz) at a libration phase of 180°. (a) disks in a meridional quarter-plane represent the location and size of the 64 chosen targets, and are colored with the value of the normalized fluid rotation rate $f_{fluid}/\Delta f$ obtained by the inversion. (b) the inversion error is colored in a similar representation. (c) $f_{fluid}/\Delta f$ as a function of cylindrical radius s for all 64 targets. At each target, the horizontal bar gives its width, while the vertical bar is the inversion error. Smoothed s-profiles (solid lines) are obtained from the targets' results at each of their 6 z-coordinate by Makima-interpolation.

5b. Figure 5c gathers the s-profiles obtained at all 6 z-lines. Value for each target is given with a horizontal bar giving the target's radius, and a vertical bar the estimated error. Smooth s-profiles computed as in section 2 are also drawn.

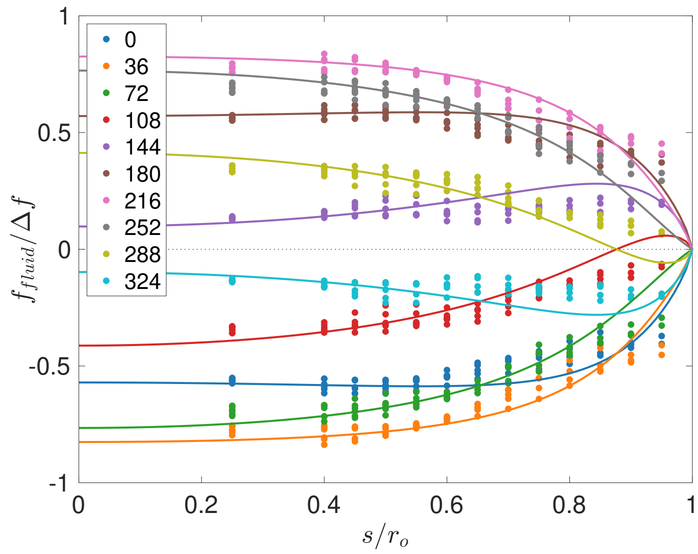

Fig. 6 2D SOLA inversion results for libration flow ($f_o = 15$ Hz, $f_{lib} = 0.05$ Hz and $\Delta f = 1.5$ Hz): normalized fluid rotation rate as a function of cylindrical radius for 10 libration phases (legend in degrees). For each libration phase, the values obtained at the 6 values of z are drawn. The color solid lines are the predictions from Greenspan's flow at each libration phase delayed by 10°.

Figure 6 gathers the fluid rotation rate f_{fluid} s-profiles obtained from the inversions at 10 libration phases. The results are very similar to those shown in Figure 3 from the 1D inversion. The 2D inversion confirms the z-invariance of the flow. The same deviations from Greenspan's predictions show up for s between 0.7 and 1.

3.2 Resolution kernels

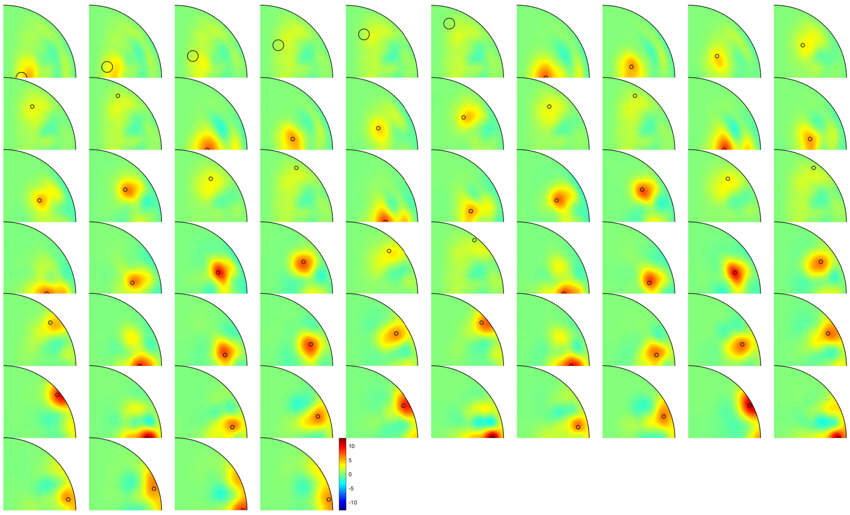

Fig. 7 Resolution kernels $A^{(k)}(r, \theta)$ for the 2D SOLA inversion of the splittings of 53 acoustic doublets. For each of the 64 targets, the amplitude of the resolution kernel is color-mapped in a meridional quarter-plane. A black circle indicates the position and radius of the target.

Resolution kernels $A^{(k)}(r, \theta)$ are displayed in Figure 7. As expected, resolution is very poor near the vertical axis. The kernels are rather well-peaked at target locations for most other targets, but their radius at mid-height is at least twice as large as the chosen target's radius, like in the 1D s-inversion. However, we observe that the 2D-inversion can clearly resolve the variation of flow rotation rate with z in most of the domain. We can thus be confident that the near-coincidence of the 6 s-profiles for each libration phase in Figure 6 is a resolved feature of the flow, in agreement with Greenspan's theory.

3.3 Data fits

As discussed in section 2.3, we need a complete model in order to compute the predicted splittings. We thus constructed a smooth model by first interpolating the target's results along s (as shown in Figure 5), and then interpolating these profiles in z. Both interpolations are performed with MATLAB®'s modified Akima (Akima 1970) interpolation. Fluid rotation rate is set to zero at the boundary ($r = 1$).

We can then compute the frequency splitting predicted by our inverted model for all 53 acoustic doublets. The fit to the data is almost identical to the fit of the 1D SOLA inversion shown in Figure 4, with $misfit = 0.70$.

4 Limitations and perspectives

Despite the excellent agreement between measured splittings and their prediction from Greenspan's flow model, as displayed in Paper 1 (apart for the observed time-delay), the retrieval of the fluid flow from these splittings appears somewhat disappointing. There is no problem with the time-variation, which is already established from the data and its sinusoidal fit. However, one might have thought that the 1D s-inversion, with only 12 targets, would fit Greenspan's profile. It is not quite the case, as shown in Figure 3.

OLA inversion methods are often presented as 'parameter-free' (e.g. see Zaroli 2019). This is true in the sense that no a priori information on the model smoothness, for example, is needed. However, there remains a choice to be made on the trade-off parameter η. All results presented so far were obtained with $\eta = 40$, for both the 1D- and 2D-inversions.

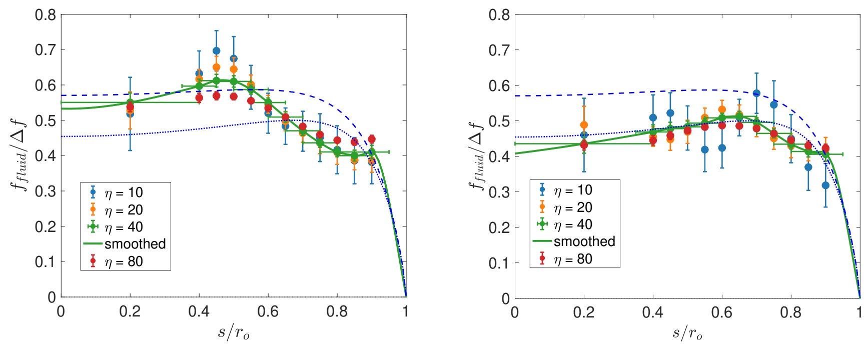

Fig. 8 Normalized fluid rotation rate as a function of cylindrical radius of target locations, from the inversion of frequency splittings at a 180° libration phase, for different values of the η parameter. The horizontal bars give the targets' width, while the vertical bars are the inversion error. The blue dotted line is Greenspan's profile at a libration phase of 180°, while the dashed blue line is the same at a phase delayed by 10°. (a) results from the inversions of measured splittings; (b) results from the inversions of synthetic splittings computed from Greenspan's model.

In Figure 8 we illustrate the impact of different choices for η, in the example of a 1D-inversion for a libration phase of 180°. Figure 8a compares the normalized fluid rotation rate obtained at our 12 s-targets for four inversions with values of η: 10, 20, 40 and 80. The smoothed profile is also shown for $\eta = 40$, together with Greenspan's profiles for a libration phase of 180° (dotted line) and 190° (dashed line). We observe that all models overestimate fluid velocity around $s = 0.5$, and underestimate it between $s = 0.6$ and 0.9. This is a consequence of the trade-offs between these two regions, which is also visible in the side lobes of the resolution kernels shown in Figure 3. Increasing η reduces the oscillation and widens the resolution kernels. It also reduces the error on the inverted model, but this error only measures the propagation of the data error in the 'weighted average' (Zaroli 2019). It does not reflect the deviation of that weighted average from the true model. The average normalized misfit only weakly depends upon η, with $misfit = 0.73$, 0.74, 0.73 and 0.83 for $\eta = 10$, 20, 40 and 80, respectively.

Deviations of the inverted models from Greenspan's flow model could be due to the ellipticity of the ZoRo shell, which is not taken into account in our sensitivity kernels. It could also be the sign of flow complexities that show up for strong enough libration (Noir et al. 2009). They could also be due to limitations of the acquisition strategies exposed in Paper 1, or to a variation of the observed time-delay with mode numbers. We don't think that it is the case, because of the excellent agreement between observed splittings and those predicted by convolving Greenspan's flow with the acoustic sensitivity kernels and also because synthetic tests display similar spurious oscillations. This is illustrated in Figure 8b, which shows profiles obtained from the inversions of synthetic splittings, predicted by Greenspan's flow model, using the same collection of modes, with their individual error, and adding a random noise within that error range. Oscillations around the true model (dotted blue line) are observed for the different values of η. The reason is to be found in the limited spatial resolution allowed by the set of 53 splittings we could measure. Figure 1 shows that individual sensitivity kernels are a bit wide, and that their complementarity is limited.

We note that we lack splitting measurements for ${}_nS_l^{\pm m}$ doublets with $m \lesssim l$. This is because their spectral peaks tend to overlap with those of neighboring doublets. For fundamental doublets ($n = 0$), spectral peaks are wide and often difficult to pick unambiguously. However, synthetic spectra computed for Greenspan's flow model do provide a good fit to these unresolved spectra. It is thus certainly feasible to obtain more information from the full frequency spectrum, or from the time-domain analysis proposed in Paper 1.

5 Conclusion

We have applied the SOLA inversion method to a set of 53 frequency splittings of acoustic doublets, acquired for several phases of a libration-driven flow, as described in Paper 1. The inversion yields fluid flow rotation rate f_{fluid} as a function of cylindrical radius s (1D-inversion) or in an (r, θ) meridional quarter-plane (2D-inversion). The retrieved values, shown in Figure 2 and 6, respectively, are in good agreement with Greenspan's solution for this libration flow (Greenspan 1968; Nataf et al. 2025). The flow amplitudes and time-variation are very well retrieved, but the exact s-profiles of f_{fluid} are not perfectly recovered. The analysis of the resolution kernels, shown in Figures 3 and 7, indicates that the data offer a good (r, θ)-resolution, but over an averaging area of $\sim 5\%$ of a meridional quarter-plane. The resolution vanishes near the vertical spin axis, and some trade-offs are present, in particular in the equatorial region. Obtaining the splittings of more ${}_nS_l^{\pm m}$ acoustic doublets, in particular with

$m \lesssim l$, should improve the resolution and the retrieval of the fluid flow. We believe that Modal Acoustic Velocimetry offers interesting prospects in fluid dynamic experiments.

Supplementary information. If your article has accompanying supplementary file/s please state so here.

Please refer to Journal-level guidance for any specific requirements.

Acknowledgments. This work was partly supported by the Programme National de Planétologie (PNP) of CNRS-INSU co-funded by CNES. ISTerre is part of Labex OSUG@2020 (ANR10 LABX56). HCN thanks Christophe Zaroli for useful comments on the SOLA inversion method.

Declarations

Some journals require declarations to be submitted in a standardised format. Please check the Instructions for Authors of the journal to which you are submitting to see if you need to complete this section. If yes, your manuscript must contain the following sections under the heading 'Declarations':

- Funding This work was partly supported by the Programme National de Planétologie (PNP) of CNRS-INSU co-funded by CNES. ISTerre is part of Labex OSUG@2020 (ANR10 LABX56).
- Conflict of interest/Competing interests (check journal-specific guidelines for which heading to use) The authors declare no conflict of interest.
- Ethics approval Not applicable.
- Consent to participate
- Consent for publication
- Availability of data and materials
- Code availability
- Authors' contributions: SS guided the use of the SOLA inversion method. HCN performed the inversions and their analysis. This article was written by HCN, with complements and review by SS.

If any of the sections are not relevant to your manuscript, please include the heading and write 'Not applicable' for that section.

Editorial Policies for:

Springer journals and proceedings: https://www.springer.com/gp/editorial-policies

Appendix A 2D sensitivity kernels

Figure A1 shows the 2D sensitivity kernels ${}_nK_l^m(r,\theta)$ for the collection of 53 acoustic doublets ${}_nS_l^{\pm m}$ inverted in this study. The ellipticity of ZoRo's shell is ignored for these kernels.

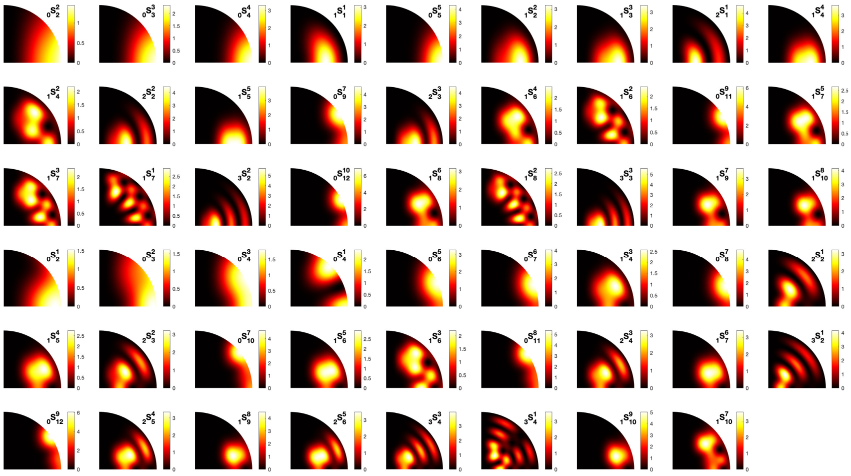

Fig. A1 Meridional map (upper half) of 2D sensitivity kernels ${}_nK_l^m(r,\theta)$ for the collection of 53 ${}_nS_l^{\pm m}$ acoustic doublets inverted in this article. Remember that all kernels are positive and symmetric with respect to the equator.

Appendix B SOLA inversion

We recall here the SOLA algorithm, closely following the rules and notations given by Zaroli (2019). The SOLA method aims at finding the *optimal unbiased weighted average* $\hat{m}^{(k)}$ of the true model $m(\mathbf{r})$ over a given target k, defined by a function $T^{(k)}(\mathbf{r})$, typically a ball centered on $\mathbf{r}^{(k)}$. For that, it minimizes a cost function:

$$\mathcal{C}^{(k)} = \int \left[A^{(k)}(\mathbf{r}) - T^{(k)}(\mathbf{r})\right]^2 d^3\mathbf{r} + \eta^2 \sigma^2_{\hat{m}^{(k)}} \tag{B1}$$

subject to the *unimodular condition*:

$$\int A^{(k)}(\mathbf{r})\, d^3\mathbf{r} = 1. \tag{B2}$$

The first term of $\mathcal{C}^{(k)}$ measures the deviation of the *averaging kernel* from the target kernel, while the second term measures the model variance, weighted by the square of the trade-off parameter η. Note that, following Zaroli (2019), we choose the same value of η for all targets k.

Because of the linear relationship between the model parameters and the measured data, one can express the optimal model we are looking for as:

$$\hat{m}^{(k)} = \sum_{i=1}^{N} x_i^{(k)} d_i, \tag{B3}$$

with N the number of measurements d_i. The inversion consists in finding the coefficients $x_i^{(k)}$ that minimize the cost function $\mathcal{C}^{(k)}$. One can then recover the weighted average $\hat{m}^{(k)}$ from equation B3, and the averaging kernel (resolution kernel) by:

$$A^{(k)}(\mathbf{r}) = \sum_{i=1}^{N} x_i^{(k)} K_i(\mathbf{r}), \tag{B4}$$

where $K_i(\mathbf{r})$ is the sensitivity kernel of the i^{th} data. The propagated model error is obtained from:

$$\sigma^2_{\hat{m}^{(k)}} = \sum_{i=1}^{N} \left(x_i^{(k)}\right)^2. \tag{B5}$$

Note that $\sigma_{\hat{m}^{(k)}}$ only measures the error brought by propagating the data errors to the model space. It is not an estimate of the true error (weighted average $\hat{m}^{(k)}$ estimate minus the 'true' model $m(\mathbf{r}^{(k)})$).

We direct the reader to section 2 of Zaroli (2019) for a detailed description of the SOLA inversion procedure that yields the requested $x_i^{(k)}$ coefficients.

In our application, the data vector d_i is the set of peak-to-peak frequency splittings obtained in Paper 1, corrected for the Coriolis splitting of the spinning shell, and normalized by their measurement error. The weighted average $\hat{m}^{(k)}$ is the inverted rotation rate f_{fluid} of the fluid flow in the spinning shell reference frame, at a given target k. The target function $T(\mathbf{r})^{(k)}$ is defined on an s-segment between $s^{(k)} - w^{(k)}$ and $s^{(k)} + w^{(k)}$ in the 1D-inversion, and on a disk of radius $w^{(k)}$ centered on an $(r, \theta)^{(k)}$ point in the 2D-inversion. In both cases, its uniform amplitude $a^{(k)}$ is set in order for $T(\mathbf{r})^{(k)}$ to satisfy the unimodular condition B2.

References

Aerts, C., Christensen-Dalsgaard, J., Kurtz, D.W.: Asteroseismology. Springer, Dordrecht Heidelberg London New York (2010)

Albo, P.G., Gavioso, R., Benedetto, G.: Modeling steady acoustic fields bounded in cavities with geometrical imperfections. International Journal of Thermophysics **31**(7), 1248–1258 (2010)

Akima, H.: A new method of interpolation and smooth curve fitting based on local procedures. Journal of the ACM **17**(4), 589–602 (1970)

Backus, G.E., Gilbert, J.: Numerical applications of a formalism for geophysical inverse problems. Geophysical Journal International **13**(1-3), 247–276 (1967)

Greenspan, H.P.: The Theory of Rotating Fluids. Cambridge Monographs on Mechanics and Applied Mathematics. Cambridge University Press, Cambridge, UK (1968)

Ledoux, P.: The nonradial oscillations of gaseous stars and the problem of Beta Canis Majoris. Astrophysical Journal **114** (1951)

Mautino, A.R.: Inverse spectral methods in acoustic normal mode velocimetry of high Reynolds number spherical Couette flows. Master's thesis, University of Maryland (2016)

Noir, J., Hemmerlin, F., Wicht, J., Baca, S.M., Aurnou, J.M.: An experimental and numerical study of librationally driven flow in planetary cores and subsurface oceans. Physics of the Earth and Planetary Interiors **173**(1-2), 141–152 (2009) https://doi.org/10.1016/j.pepi.2008.11.012

Nataf, H.-C., Roux, P., Su, S., Cardin, P., Cébron, D., Do, Y.: Modal Acoustic Velocimetry in libration-driven flows - Part 1 : Acquisition strategies. to be submitted (2025)

Pijpers, F., Thompson, M.: Faster formulations of the optimally localized averages method for helioseismic inversions. Astronomy and Astrophysics **262**(2), 33–36 (1992)

Pijpers, F., Thompson, M.: The SOLA method for helioseismic inversion. Astronomy and Astrophysics **281**, 231–240 (1994)

Su, S.: Modal Acoustic Velocimetry in a gas–filled rotating spheroid. Theses, Université Grenoble Alpes [2020-....] (February 2020). https://theses.hal.science/tel-02612799

Triana, S.A., Zimmerman, D.S., Nataf, H.-C., Thorette, A., Lekic, V., Lathrop, D.P.: Helioseismology in a bottle: Modal Acoustic Velocimetry. New Journal of Physics **16**(11), 113005 (2014)

Zaroli, C.: Seismic tomography using parameter-free Backus–Gilbert inversion. Geophysical Journal International **218**(1), 619–630 (2019)